Detailed ferromagnetic resonance study of amorphous Fe-rich $Fe_{90-x}Co_xZr_{10}$ alloys. I: re-entrant behaviour and low-lying magnetic excitations

1996 J. Phys.: Condens. Matter 8 4545

(http://iopscience.iop.org/0953-8984/8/25/012)

J. Phys.: Condens. Matter **8** (1996) 4545–4565. Printed in the UK

Detailed ferromagnetic resonance study of amorphous Fe-rich $Fe_{90-x}Co_xZr_{10}$ alloys. I: re-entrant behaviour and low-lying magnetic excitations

V Siruguri† and S N Kaul‡

School of Physics, University of Hyderabad, Central University PO, Hyderabad-500 046, India

Received 4 January 1996

Abstract. Results of exhaustive ferromagnetic resonance (FMR) measurements performed on amorphous (a-)$Fe_{90-x}Co_xZr_{10}$ ($0 \leqslant x \leqslant 18$) alloys at temperatures ranging from 10 to 500 K are presented and discussed in the light of existing theoretical models. The peak-to peak FMR linewidth ΔH_{pp} consists of two contributions: one originating from two-magnon and multiple-magnon scattering processes and the other arising from the Laundau–Lifshitz–Gilbert damping mechanism. ΔH_{pp} for the alloys with $x \leqslant 2$, as in other re-entrant (RE) systems, increases *exponentially* as the temperature is lowered through the RE transition temperature T_{RE}. The Landé splitting factor is independent of both temperature and Co concentration, whereas the Gilbert damping parameter is temperature-independent but decreases with increasing x. For all the alloys in question, thermal demagnetization is mainly due to spin-wave (SW) excitations and the SW stiffness coefficient D renormalizes with temperature in accordance with the predictions of the itinerant-electron model. SW modes in the alloys with $x \leqslant 2$ soften at $T \lesssim T_{RE}$ and D possesses a reduced but finite value in the RE state. Competing interactions present in the parent alloy a-$Fe_{90}Zr_{10}$ confine the direct exchange interactions (DEIs) to the nearest neighbours only and partial replacement of Fe with Co progressively tilts the balance in favour of ferromagnetic interactions between Fe spins with the result that DEIs now involve next-nearest neighbours too and the divergence in $\Delta H_{pp}(T)$ at low temperatures is completely suppressed for $x > 4$.

1. Introduction

Considerable scientific attention has been devoted in the recent years to the spin systems that exhibit re-entrant (RE) behaviour at low temperatures. The phenomenon of re-entrance manifests itself in a transition from the paramagnetic (PM) state to the ferromagnetic (FM) or antiferromagnetic (AF) state at a critical temperature T_C (the Curie temperature) or T_N (the Neél temperature) which at a lower temperature T_{RE} is followed by another transition from the FM or AF state to a spin-glass (SG)-like (RE) state. Like many other RE systems investigated in the past, amorphous (a-)$Fe_{90-x}Co_xZr_{10}$ alloys with $x \leqslant 2$ enter into a state with long-range FM ordering at T_C as the temperature is lowered through T_C and exhibit a strong irreversibility [1, 2] in the low-field thermomagnetic scans at $T \lesssim T_{RE}$ (which lies well below T_C) that is reminiscent of SG behaviour. Our recent Mössbauer data [3] on the parent alloy a-$Fe_{90}Zr_{10}$ have indicated that the transition at T_{RE} is not well defined and the RE state is a mixed state in which long-range FM order coexists with cluster SG order.

† Present address: Inter University Consortium—Bombay Centre, Solid State Physics Division, Bhabha Atomic Research Centre, Trombay, Bombay-400 085, India.

‡ Author to whom all correspondence should be addressed.

0953-8984/96/254545+21$19.50

In view of this observation, a systematic study of the alterations in the nature of magnetic ordering brought about by a partial substitution of Fe by Co in the a-$Fe_{90-x}Co_xZr_{10}$ alloy series is highly desirable.

The nature of low-lying magnetic excitations in a-$Fe_{90+y}Zr_{10-y}$ ($0 \leqslant y \leqslant 3$) alloys has lately given rise to much controversy. While Krishnan *et al* [4] found that the 'in-field' magnetization varies with temperature as $M(H,T) \propto T^{3/2}$ for $T > T^*(H)$ in external magnetic fields up to 140 kOe for a-$Fe_{90}Zr_{10}$ and that the spin-wave (SW) stiffness coefficient D *increases* with increasing H, attaining a maximum value of 39.1 meV Å^2, Beck and Kronmüller [5] observed that the thermal demagnetization in the temperature range 4.2 K $\lesssim T \lesssim 0.5T_C$ is solely due to Stoner single-particle (SP) excitations (SW excitations) for $H < 2.7$ kOe ($H > 2.7$ kOe) and D *decreases* from 50 to 35 meV Å^2 as H is increased from 2.7 to 40 kOe. The observation based on inelastic neutron scattering (INS) experiments on a-$Fe_{91}Zr_9$, that no propagating features [6] were evident at any temperature below T_C for the wavevector transfer range 0.05 Å$^{-1} \leqslant q \leqslant 0.12$ Å^{-1}, complicated the issue further. In contrast with the above findings, the recent high-resolution bulk magnetization data of Kaul [7] revealed that, besides local spin-density fluctuations, both SW and SP excitations contribute to thermal demagnetization in a-$Fe_{90+y}Zr_{10-y}$ alloys and D has a *field-independent* value of 32 ± 1 (29 ± 1) meV Å^2 for a-$Fe_{90}Zr_{10}$ (a-$Fe_{91}Zr_9$). Within the framework of the model of infinite FM matrix plus finite FM clusters [8–10], Kaul [7] offered a straightforward explanation for the absence of SW peaks in the INS scans [11] taken in the above-mentioned q-range and suggested that INS measurements should be extended to sufficiently low q-values so as to detect SW peaks corresponding to long-wavelength magnons excited in the infinite FM matrix. Subsequently, the existence of well defined SW excitations in a-$Fe_{90-x}Ni_xZr_{10}$ alloys with $1 \leqslant x \leqslant 20$ was revealed by the INS scans taken at $T \lesssim T_C$ in the q-range 0.04 Å$^{-1} \leqslant q \leqslant 0.1$ Å^{-1}. The existence of well defined SWs and enhancement of the Fe moment in such alloys is thought to be the result of the increase in the number of ferromagnetically coupled Fe spins at the expense of those antiferromagnetically coupled as Ni partly replaces Fe in the parent alloy a-$Fe_{90}Zr_{10}$. Since Ni and Co play similar roles so far as the Fe moment enhancement is concerned, results of a systematic investigation of low-lying magnetic excitations in a-$Fe_{90-x}Co_xZr_{10}$ alloys should provide a means of testing whether or not the above interpretation is correct.

Detailed ferromagnetic resonance (FMR) measurements have been performed on a-$Fe_{90-x}Co_xZr_{10}$ alloys with $0 \leqslant x \leqslant 18$ over a wide temperature range 10 K $\leqslant T \leqslant$ 500 K with a view to monitoring the changes in magnetic ordering caused by the alterations in the temperature and Co concentration. The FMR technique is well suited to this type of study because the FMR linewidth is extremely sensitive to the kind of magnetic order present in the system. The $M(H,T)$ data, deduced from FMR spectra through an elaborate lineshape analysis, have been analysed so as to determine the contributions to thermal demagnetization arising from SW and SP excitations and to arrive at a reliable estimate of the SW stiffness coefficient D.

2. Experimental details

Amorphous $Fe_{90-x}Co_xZr_{10}$ ($0 \leqslant x \leqslant 18$) alloys were prepared in the form of ribbons (1–2 mm in width and 30–40 μm in thickness) under a helium atmosphere by the single-roller melt-quenching technique. The amorphous nature of the ribbons thus fabricated was confirmed by the x-ray diffraction and high-resolution electron microscopy methods. No traces of either surface crystallization or a second minor crystallographic phase were

revealed. The field derivative dP/dH of the microwave power P absorbed during the FMR process was measured as a function of the external static magnetic field H on strips 4 mm long, cut from the alloy ribbons, using horizontal-parallel ($\|^h$) and vertical-parallel ($\|^v$) sample configurations (in which the external field H lies in the ribbon plane and is directed along the length and breadth, respectively), at a fixed microwave frequency of about 9.23 GHz on a JEOL FE3X ESR spectrometer in the temperature range 77–500 K. The sample temperature was varied between 100 and 300 K by regulating the flow of cold nitrogen gas. A proper gas flow was achieved by controlling the power input to a heater, immersed in a liquid-nitrogen (LN_2) container, with the aid of a proportional, integral and derivative temperature controller. The controlling sensor used was a pre-calibrated copper–constantan thermocouple situated just outside the microwave cavity. The temperature at the sample site was monitored by another pre-calibrated copper–constantan thermocouple in close contact with the sample. The temperature stability achieved at the sample site was better than ± 50 mK. Measurement at 77 K was performed by dipping the sample in a special LN_2 Dewar. The sample temperature was varied from 300 to 500 K by heating air blown through the cavity by a compressor. Low-temperature FMR measurements extending down to 10 K were also performed using a Bruker ESP100 ESR spectrometer at Bhabha Atomic Research Centre, Bombay. A closed-cycle refrigerator was coupled to the spectrometer in order to attain low temperatures. The temperature stability achieved was better than ± 25 mK and the measurements were taken at fixed temperature values after the sample had been cooled to the lowest temperature in zero external field or in an external field of 3 kOe. As the present amorphous alloys are extremely sensitive to stress, it is imperative to ensure that the samples do not experience any stress during measurement. An appropriate sample mounting technique [12], which ensures high reproducibility of the data by getting rid of spurious stress-induced effects, was used for measurements. Since the microwave field at 9.23 GHz penetrates a surface layer of thickness about 1 μm, it is imperative to ascertain whether the observed resonances are characteristic of the bulk. In order to verify this, the samples were either etched in Nital solution (10% HNO_3 + 90% ethanol) or mechanically polished and then power absorption derivative (PAD) curves were recorded. These experiments [13] demonstrated that the observed resonances were indeed characteristic of the bulk and did not originate from the surface layer.

3. Data analysis and results

3.1. Lineshape analysis

The observed functional dependence of dP/dH on H in the horizontal-parallel ($\|^h$) configuration is depicted in figure 1 for three ranges of temperatures for a-$Fe_{90}Zr_{10}$. Each of the figures 1(a)–1(c) displays the PAD curves for a few selected values of temperatures in the low-temperature (10 K $\leqslant T \leqslant T_{RE}$), intermediate-temperature ($T_{RE} \leqslant T \leqslant T_C$) and high-temperature ($T > T_C$) ranges, where T_{RE} is the so-called RE transition temperature and T_C the Curie temperature. These PAD curves are representative of those recorded for other compositions in the same series in both $\|^h$ and $\|^v$ (vertical-parallel) geometries. It is clear from figures 1(a) and 1(b) that the dP/dH curves in the low- and intermediate-temperature ranges consist of a single resonance (henceforth referred to as the primary or main resonance) line which shifts to higher fields as the temperature is increased. This resonance broadens at a rapid rate for $T \geqslant 0.8T_C$. Apart from this resonance, the signature of a secondary resonance at a lower field value $H_{res}^{\prime\|^h} = H_{res}^{\prime\|^v} \simeq 850$ Oe is first noticed at $T \simeq T_C$ in the most sensitive setting of the spectometer (figure 1(c)). This secondary

resonance, observed earlier [14] in the case of a-$Fe_{90-x}Zr_{10+x}$ alloys as well, becomes better resolved as the temperature is increased beyond $T_C + 10$ K. In this paper, only the results pertaining to the primary resonance are discussed. The physical origin and properties of the secondary resonance will form the subject of a forthcoming paper. The physical quantities deduced from the dP/dH curves are the resonance field H_{res} (defined as the field where the $dP/dH = 0$ line cuts the dP/dH versus H curve) and the peak-to-peak linewidth ΔH_{pp} (defined as the field difference between the extrema of the dP/dH versus H curve). Now that the peak-to-peak linewidth ΔH_{pp} forms an appreciable fraction of the resonance field H_{res} for the alloys in question, the observed value of H_{res} could significantly differ from the actual ('true') resonance line centre. This necessitated a complete lineshape calculation for each resonance line separately. Such a calculation consists in fitting the dP/dH versus H curves recorded at different temperatures in the $\|^h$ configuration to the theoretical expression [14, 15]

$$\frac{dP_{\|}}{dH} \propto \frac{d}{dH}[(\mu'^2 + \mu''^2)^{1/2} + \mu'']^{1/2} \tag{1}$$

with real and imaginary components of the dynamic permeability given by

$$\begin{aligned}\mu' = \{&[(H + H_k)(B + H_k) - \Gamma^2 - (\omega/\gamma)^2][(B + H_k)^2 - \Gamma^2 - (\omega/\gamma)^2] \\ &+2\Gamma^2(B + H_k)(B + H + 2H_k)\}\{[(H + H_k)(B + H_k) - \Gamma^2 - (\omega/\gamma)^2]^2 \\ &+\Gamma^2(B + H + 2H_k)^2\}^{-1}\end{aligned} \tag{2a}$$

$$\begin{aligned}\mu'' = \{&-2\Gamma(B + H_k)[(H + H_k)(B + H_k) - \Gamma^2 - (\omega/\gamma)^2] \\ &+\Gamma(B + H + 2H_k)[(B + H_k)^2 - \Gamma^2 - (\omega/\gamma)^2]\}\{[(H + H_k)(B + H_k) \\ &-\Gamma^2 - (\omega/\gamma)^2]^2 + \Gamma^2(B + H + 2H_k)^2\}^{-1}\end{aligned} \tag{2b}$$

with the aid of a non-linear least-squares (LS) fit computer program. This program treats the Landé splitting factor g and saturation magnetization M_S as free-fitting parameters and makes use of the observed values of ΔH_{pp} ($= 1.45\lambda\omega/\gamma^2 M_S$) and the values of H_k derived from the expression [14, 16]

$$H_k \simeq (H_{res}^{\|^v} - H_{res}^{\|^h})/2 \tag{3}$$

which holds when $H_k \ll 4\pi M_S$. In equations (1)–(3), $B = H + 4\pi M_S$, $\Gamma = \lambda\omega/\gamma^2 M_S$, H_k is the 'in-plane' uniaxial anisotropy field, $\gamma = ge/2mc$ is the magnetomechanical ratio and λ is the Gilbert damping parameter. $H_{res}^{\|^h}$ and $H_{res}^{\|^v}$ are the resonance fields obtained after correcting the resonance fields observed in the $\|^h$ and $\|^v$ configurations, respectively, for the demagnetizing fields $H_{dem}^{\|^h}$and $H_{dem}^{\|^v}$ which have been determined earlier from the low-field magnetization measurements on the same samples with the external magnetic field applied along the easy ($\|^h$) and hard ($\|^v$) directions in the ribbon plane. The theoretical fits so obtained, denoted by open circles in figures 1(*a*)–1(*c*), determine the parameters g and M_S to an accuracy of 1% and 2%, respectively, and indicate that the Landau–Lifshitz–Gilbert (LLG) equation adequately describes the resonant behaviour of the alloys in question over the entire temperature range covered in the present experiments. In addition, the lineshape analysis reveals that the splitting factor g has a temperature-independent value of 2.07 ± 0.02 for all the alloy compositions. It is also revealed that the correction to the observed values of H_{res} at different temperatures due to finite linewidth is negligibly small at all temperatures and falls well within the uncertainty limits of $H_{res}(T)$. This result is consistent with the observation that the experimental values of $H_{res}^{\|^h}$ and $H_{res}^{\|^v}$ satisfy the resonance conditions [14, 15]

$$[(\omega/\gamma)^2 + \Gamma_{\|_h}^2] = (H_{res}^{\|^h} + 4\pi M_S + H_k)(H^{\|^h} + H_k) \tag{4a}$$

and

$$[(\omega/\gamma)^2 + \Gamma_{\|_v}^2] \simeq (H_{res}^{\|^v} + 4\pi M_S - H_k)(H^{\|^v} - H_k) \tag{4b}$$

which have been obtained by solving the LLG phenomenological equation of motion for dynamic magnetization, i.e.

$$\frac{\mathrm{d}\boldsymbol{M}}{\mathrm{d}t} = -\gamma(\boldsymbol{M} \times \boldsymbol{H}_{eff}) + \frac{\lambda}{\gamma M_S^2}\left(\boldsymbol{M} \times \frac{\mathrm{d}\boldsymbol{M}}{\mathrm{d}t}\right) \tag{5}$$

for the $\|^h$ and $\|^v$ sample configurations. In equation (5), $\boldsymbol{H}_{eff}$ is the effective magnetic field 'seen' by the spins.

3.2. Resonance field

The resonance field H_{res} deduced from the lineshape analysis for the $\|^h$ configuration is depicted in figure 2 as a function of reduced temperature T/T_C for a-$Fe_{90-x}Co_xZr_{10}$ alloys. Since the observed variation in the various physical quantities in the case of the $\|^h$ configuration is representative of the $\|^v$ configuration, the results pertaining to the $\|^h$ configuration only are discussed. Moreover, the superscript $\|^h$ is dropped for convenience. Figure 3 depicts the variation in H_{res} with T in the low-temperature region (10 K $\leqslant T \leqslant$ 200 K) for a few selected compositions. Since the conditions $H_k \ll 4\pi M_S$ and $\Gamma \ll \omega/\gamma$ are satisfied for the alloys in question, the functional dependence of H_{res} on temperature is primarily governed by $M_S(T)$. It is observed that $H_{res}(T)$ exhibits a slow increase up to $T \simeq 0.8T_C$ and then increases steeply with further increase in temperature, a direct consequence of the fact that M_S falls sharply as $T \to T_C$. At very low T, H_{res} decreases faster with decreasing temperature than can be ascribed to an increase in magnetization in the case of the $x = 0$ and 1 samples. This behaviour has been observed earlier in RE glassy systems [17] and has been attributed to the high anisotropy fields that develop in the RE state. Figure 4 shows the variation in H_{res} with Co concentration x at different T/T_C-values. In general, there is a decrease in H_{res} with increasing Co concentration. For $x \leqslant 6$, H_{res} decreases at a rapid rate whereas this rate of decrease slows down for $x > 6$ such that H_{res} has a value of 725 Oe for $x = 10$ at $0.5T_C$.

3.3. Linewidth

The variation in the 'peak-to-peak' linewidth ΔH_{pp} with reduced temperature T/T_C in the $\|^h$ configuration is depicted in figure 5 for a-$Fe_{90-x}Co_xZr_{10}$ alloys. For $T \leqslant 0.8T_C$, ΔH_{pp} for these compositions, except for $x = 0$, exhibits a weak increase with decreasing temperature whereas, for $T \geqslant 0.8T_C$, ΔH_{pp} increases steeply with increasing temperature. Frequency-dependent studies of the FMR in amorphous ferromagnets [18–20] have revealed that ΔH_{pp} consists of a frequency-independent part ΔH_0 (also called the 'zero-frequency' term) and a frequency-dependent part ΔH_{LLG} described by the empirical equation

$$\Delta H_{pp}(\nu, T) = \Delta H_0(T) + \Delta H_{LLG}(\nu, T). \tag{6}$$

In equation (6), the second term represents the LLG contribution, which is proportional to $(2\pi\lambda/\gamma^2 M_S)\nu$. However, the origin of the first term, which manifests itself as a non-zero intercept at $\nu = 0$, appears to be more complicated. Spano and Bhagat [20] attribute this additional contribution to the magnetic inhomogeneities present in amorphous ferromagnets due to topological and/or chemical short-range order. These workers empirically model the inhomogeneity by a Gaussian distribution of local magnetization and of internal dipolar fields and then calculate the linewidths that result from such a distribution. A different

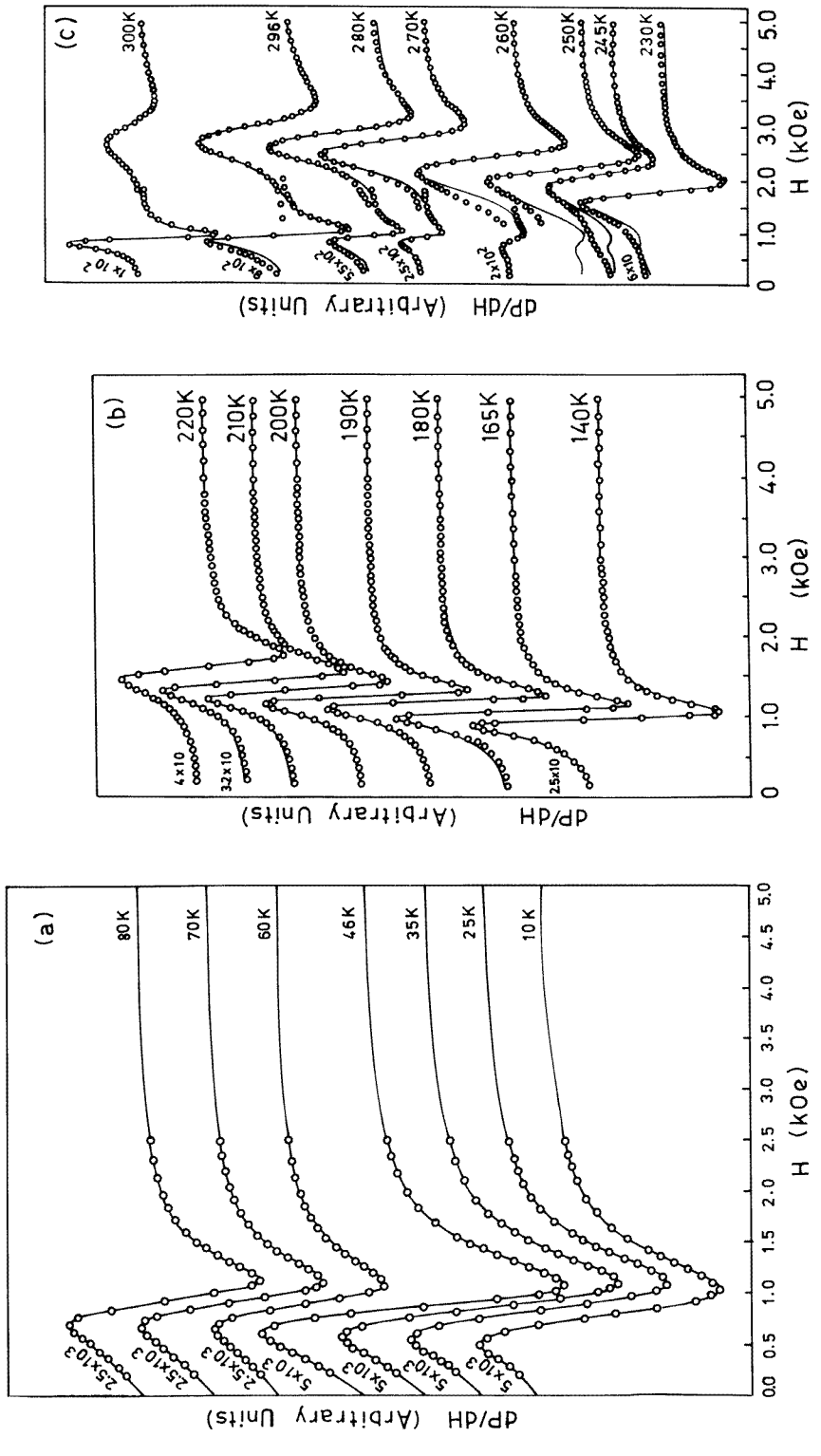

Figure 1. PAD curves for a-$Fe_{90}Zr_{10}$ alloy (*a*) in the low-temperature range, (*b*) in the intermediate-temperature range and (*c*) in the temperature region around T_C and above, recorded in the horizontal-parallel sample configuration. Solid curves depict the observed variation of dP/dH with H whereas the open cicles denote the calculated values based on equations (1)–(3) of the text. The numbers on the left-hand side of the PAD curves denote the sensitivity at which the spectra were recorded.

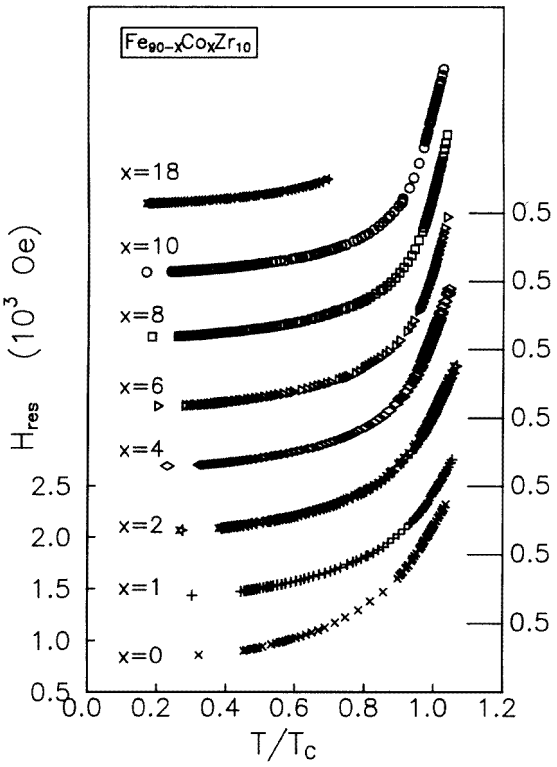

Figure 2. Variations in the resonance field H_{res} with reduced temperature T/T_C for a-$Fe_{90-x}Co_xZr_{10}$ alloys. Note that the sensitivities of the ordinate scale for all the compositions are the *same* as indicated on the left-hand side for the alloy with $x = 0$ and that the long bars on the right ordinate scale mark the starting points (corresponding to $H_{res} = 500$ Oe) of the ordinate scales for the alloys with $x = 1, 2, 4, 6, 8, 10, 18$.

approach has been taken by Cochran *et al* [21] based on FM antiresonance measurements, according to which ΔH_0 has its origin in the two-magnon scattering mechanism. The two-magnon scattering may be caused by spatial inhomogeneities in the local magnetic anisotropy fields and/or inhomogeneities in the local exchange interaction [22]. Cochran *et al* [22] found that the calculated two-magnon linewidth is proportional to M_S in agreement with the observations. An unambiguous determination of the two contributions in equation (6) necessitates the measurement of ΔH_{pp} at different microwave field frequencies from which the zero-frequency intercept is obtained. Such an analysis was not possible in the present case since the measurements were performed at a single microwave frequency (about 9.23 GHz). Nevertheless, an attempt has been made to estimate the values of λ and ΔH_0 in equation (6) through a LS fit analysis in which the approach due to Cochran *et al* [21] has been adopted by writing ΔH_0 as

$$\Delta H_0(T) = \Delta H_0' + aM_S(T) + bM_S^2(T) \tag{7}$$

where $\Delta H_0'$ is a constant, the second term is due to two-magnon scattering processes and the third *presumably* originates from multiple-magnon scattering processes. LS fits to the $\Delta H_{pp}(T)$ data based on equations (6) and (7) have been attempted in the temperature range from 77 K (100 K) to $T_C + 15$ K for alloys with $x = 1$ to 10 ($x = 0$) treating λ, ΔH_0, a and

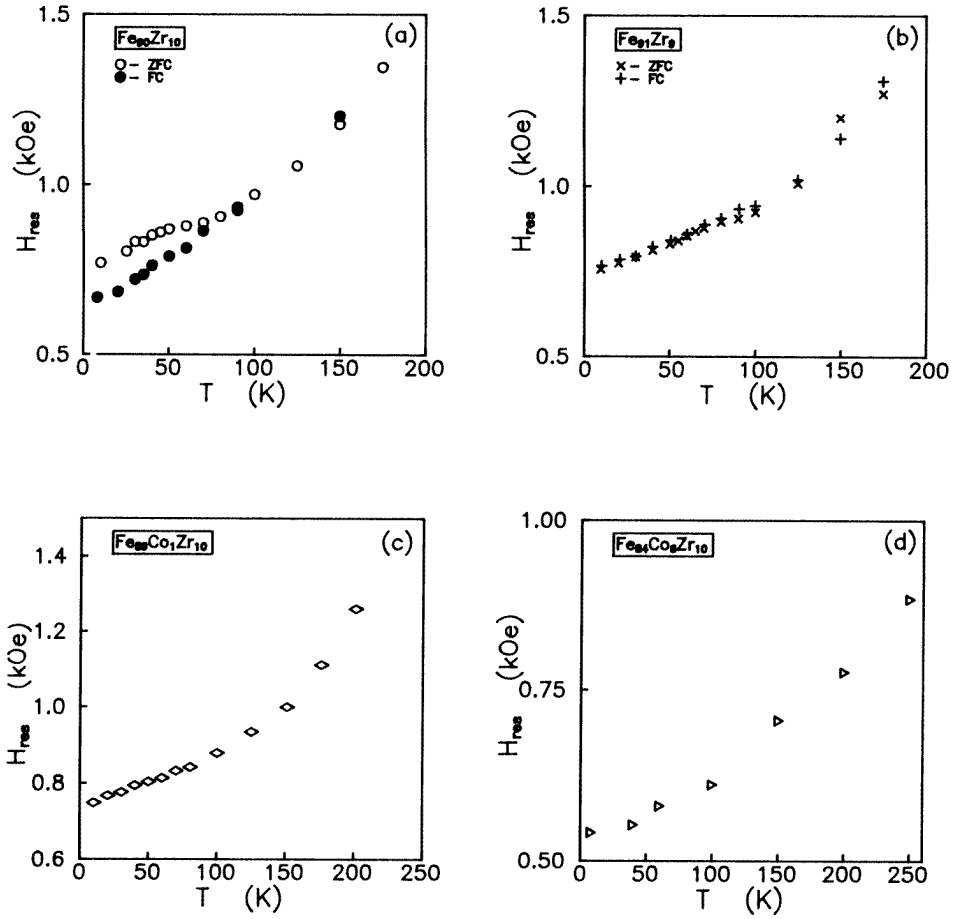

Figure 3. Temperature dependence of H_{res} in the low-temperature region for a few compositions in the a-$Fe_{90-x}Co_xZr_{10}$ alloy series and a-$Fe_{91}Zr_9$.

b as free-fitting parameters and using the M_S-values obtained from the lineshape analysis to optimize agreement with the experimental data. The solid lines through the ΔH_{pp} versus T data (figure 5) represent the best LS fits so obtained. The main findings are that

(i) the constant term $\Delta H_0'$ has a value close to zero,

(ii) the term linear in M_S contributes significantly to ΔH_0 only in the case of alloys with $0 \leqslant x \leqslant 2$ (for $x > 2$, this term (second term in equation (7)) makes little or even no contribution to ΔH_0),

(iii) the M_S^2 term gives a sizable contribution in the temperature range from 77 K to $0.8T_C$ for all the compositions studied and

(iv) The damping parameter λ is independent of temperature (since its value does not depend on the temperature range chosen for the fit) in the entire temperature range (which also includes the critical region) for all x.

While ΔH_0 does not show an systematic trend with Co concentration, the value of λ is reduced from 5.1×10^8 s^{-1} for the $x = 0$ alloy to 2.1×10^8 s^{-1} for the alloy with $x = 10$

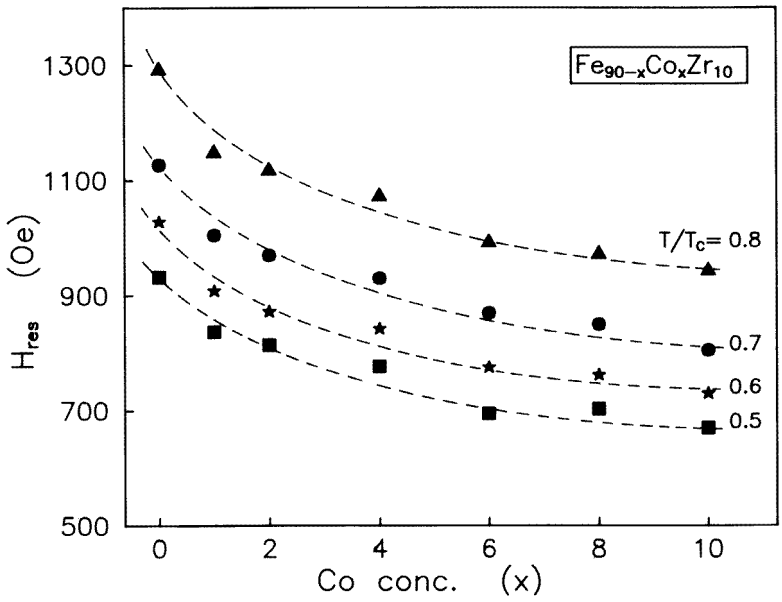

Figure 4. Co concentration dependence of H_{res} at a few representative values of the reduced temperature T/T_C.

(figure 6).

At low temperatures (10 K $\leqslant T \leqslant$ 200 K), a substantial increase in ΔH_{pp} upon lowering the temperature occurs for alloys with $x \leqslant 4$. Figure 7 shows ΔH_{pp} plotted against T in the range 10 K $\leqslant T \leqslant$ 250 K for a few selected compositions which have been reported [1, 2] to exhibit SG-like behaviour at low temperatures. The rapid increase in linewidth at low T has been observed in a number of concentrated SGs and RE systems [14, 17, 20, 23, 24] when the temperature is decreased below about $3T_{SG}$ and about $2T_{RE}$, respectively. Bhagat *et al* [25] have shown that this rapid increase can be described by an empirical relation of the form

$$\Gamma(x, \nu, T) = \Gamma_0(x, \nu) + \Gamma_1(x, \nu)(T/T_0(x, \nu))^n \exp(-T/T_0(x, \nu)) \tag{8}$$

where Γ_1 and T_0 are material parameters and Γ_0 is the value of the linewidth in the intermediate-temperature region where it has a constant value or is weakly dependent on temperature. The exponent n equals 1 or 0 depending upon whether or not the linewidth goes through a maximum at low temperatures. The solid curves through the data points in figure 7 are LS fits to the data based on equation (8). In these fits, Γ_0, Γ_1 and T_0 are treated as free-fitting parameters while n is set equal to unity. From figure 7 it is observed that equation (8) provides a reasonably good fit to the data. Such LS fits to the data for a-$Fe_{90}Zr_{10}$ (a-$Fe_{89}Co_1Zr_{10}$) alloy gave the values $\Gamma_0 = 334.7$ Oe (236.7 Oe), $\Gamma_1 = 257$ Oe (321 Oe) and $T_0 = 31.1$ K (48.2 K). The maxima at low temperatures in $\Delta H_{pp}(T)$ are characteristic of many RE systems [20, 23, 26]. The data presented in figure 7 also demonstrate that the upturn in $\Delta H_{pp}(T)$ at low T is completely absent for the alloy with $x = 6$ and the linewidth is nearly independent of temperature for $T \ll T_C$.

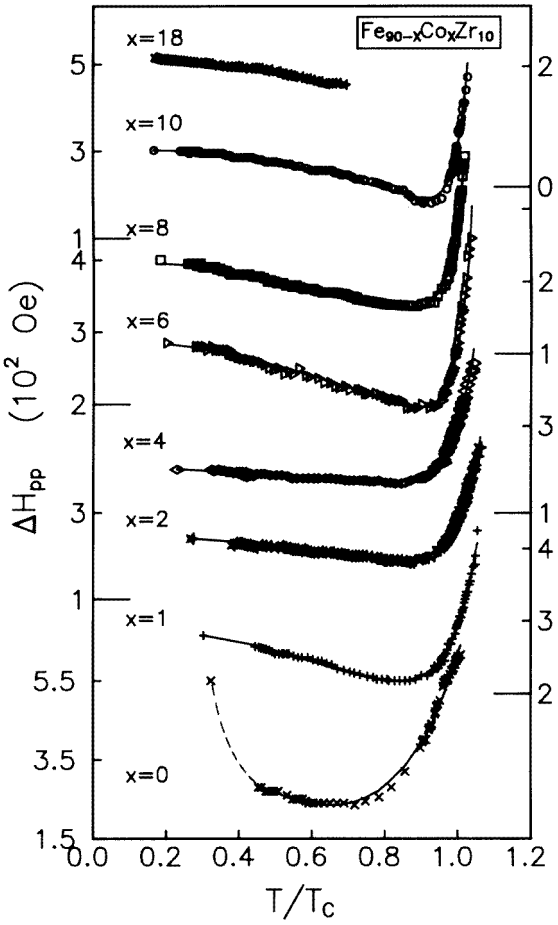

Figure 5. Dependence of the 'peak-to-peak' linewidth ΔH_{pp} on the reduced temperature T/T_C for a-$Fe_{90-x}Co_xZr_{10}$ alloys. Note that the ordinate scales on the left are for $x = 0$, 2, 6 and 10 whereas those on the right are for $x = 1$, 4, 8 and 18; the longer horizontal bars mark the starting points of these scales.

3.4. Low-lying magnetic excitations

Values of saturation magnetization M_S have been determined to a high precision from the lineshape analysis. Such values of M_S are plotted against temperature T in figure 8. In view of the fact that there exist widely divergent viewpoints concerning the nature of low-lying magnetic excitations in Fe-rich a-Fe–Zr alloys, we have analysed the $M_S(T)$ data so as to determine the contributions arising from SW and SP excitations to the thermal demagnetization and arrive at a reliable estimate of the SW stiffness coefficient D. In this regard, it must be emphasized that the present $M(H, T)$ data deduced from FMR spectra, even under the most favourable conditions, cannot match the accuracy of bulk magnetization (BM) data. Nevertheless, the precision in the deduced $M(H, T)$ data suffices to determine the dominant contributions to thermal demagnetization with reasonable accuracy. The contributions due to SW and SP excitations to the thermal demagnetization of 'in-field'

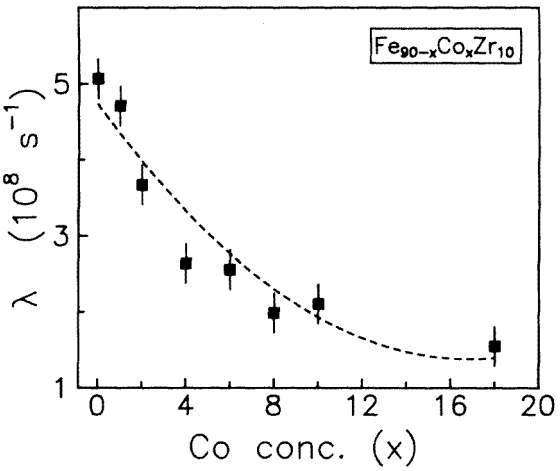

Figure 6. Co concentration dependence of the LLG damping parameter λ. The broken curve through the data points is a guide to the eye.

magnetization, i.e. $[M(H,0) - M(H,T)]/M(H,0) \equiv \Delta m$, are given by [27, 28]

$$\Delta m = \Delta m_{SW} + \Delta m_{SP} \tag{9}$$

where

$$\Delta m_{SW} = \frac{g\mu_B}{M(H,0)}\left[Z(\tfrac{3}{2}, t_H)\left(\frac{k_BT}{4\pi D(T)}\right)^{3/2} + 15\pi\beta Z(\tfrac{5}{2}, t_H)\left(\frac{k_BT}{4\pi D(T)}\right)^{5/2}\right] \tag{10}$$

is the SW contribution, and

$$\Delta m_{SP} = S(H)T^{3/2}\exp(-\Delta/k_BT) \qquad \text{(for a strong itinerant ferromagnet)} \tag{11a}$$

$$\Delta m_{SP} = S(H)T^2 \qquad \text{(for a weak itinerant ferromagnet)} \tag{11b}$$

is the SP contribution. In equation (10), the Bose–Einstein integral functions

$$Z(s, t_H) = \sum_{n=1}^{\infty} n^{-s}\exp(-nt_H) \tag{12}$$

with

$$t_H = T_g/T = g\mu_B H_{eff}/k_BT \tag{13}$$

allow for the extra energy gap $g\mu_B H_{eff}$ $(= k_BT_g)$ in the SW spectrum arising from the effective field

$$H_{eff} = H - 4\pi NM + H_k \tag{14}$$

(where N, M and H_k are the demagnetizing factor, magnetization and anisotropy field, respectively) which the spins experience within the sample. Alternatively, in the presence of the external magnetic field H, the magnon dispersion relation takes the form

$$E_q(T) = \hbar\omega_q(t) = g\mu_B H_{eff} + D(T)q^2(1 - \beta q^2) \tag{15}$$

where the coefficient β, is related to the mean-square range $\langle r^2\rangle$ of the exchange interaction as $\langle r^2\rangle = 20\beta$ and D renormalizes with temperature according to the relations [7, 29]

$$D(T) = D(0)(1 - D_2T^2) \tag{16}$$

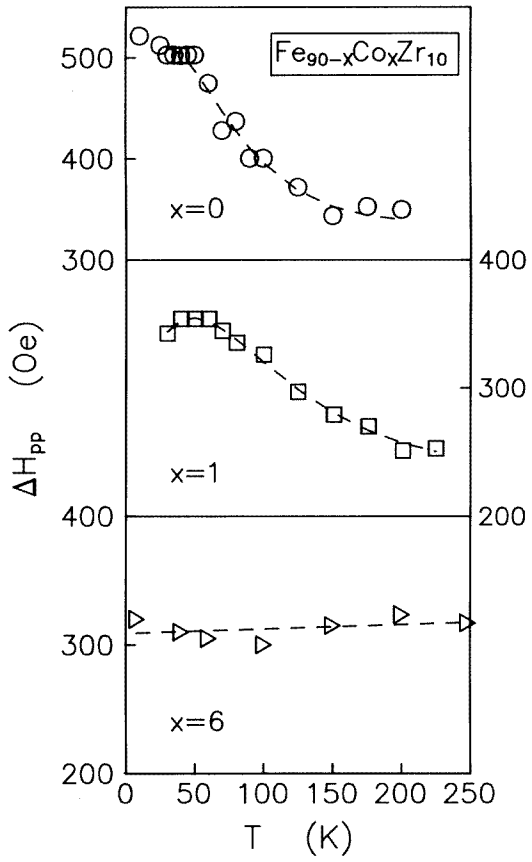

Figure 7. Variation in ΔH_{pp} in the low-temperature region for a few representative alloy compositions. The broken curves through the data points represent the best LS fits based on equation (8) of the text with the value $n = 1$.

and

$$D(T) = D(0)(1 - D_{5/2}T^{5/2}) \tag{17}$$

in the case of the itinerant- and localized-electron models, respectively. The demagnetization factor N in equation (14) has been determined from earlier low-field magnetization data and the splitting factor g ($= 2.07 \pm 0.02$) and H_k from FMR spectra. Theoretical LS fits to the Δm data based on equations (9)–(14) with the temperature dependence of the SW stiffness coefficient in equation (10) described either by equation (16) or by equation (17), have been attempted. When the LS fit involving six parameters, i.e. $M(H, 0)$, $D(0)$, D_2 or $D_{5/2}$, β, S and Δ, yielded the result $\Delta/k_B = 0 \pm 1$ K, equations (9), (10) and (11*b*) involving the combinations $D(T) = D(0)$, $D(T) = D(0)\ (1 - D_2T^2)$ and $D(T) = D(0)\ (1 - D_{5/2}T^{5/2})$ with either $\beta = S = 0$ or $\beta \neq 0$, $S = 0$, or $\beta = 0$, $S \neq 0$, have been used for the subsequent fits. In order to ascertain the relative importance of the SW and SP contributions to Δm within the temperature range covered in the present experiments, a 'range-of-fit' analysis has been carried out in which the values of the free fitting parameters in the above-mentioned theoretical fits are monitored as the temperature interval $t_{min} \leqslant t = T/T_C \leqslant t_{max}$ is progressively broadened by keeping t_{min} fixed at 0.4 (0.3) and varying t_{max} from 0.5 (0.4)

to 0.95 ($t^*(x)$ in case of alloys with $x = 0$, 1 and 2 ($x \geqslant 4$)). The 'range-of-fit' analysis in which t_{min} is varied while keeping t_{max} fixed at some value has also been carried out. The results of this exercise reveal that the observed variation in Δm with T over the entire temperature range is best described by the fit which is based on equations (9)–(14) and sets $\beta = S = 0$ with $D(T)$ given by equation (16) indicating that the SW excitations are *mainly* responsible for the thermal demagnetization. It has also been observed that, regardless of the temperature range chosen for the fit, inclusion of the SP contribution (the T^2 term) or the higher-order SW term ($T^{5/2}$) besides the $T^{3/2}$ term in equations (9) and (10) leaves the values of the parameters of the $T^{3/2}$ LS fit (i.e. the fit that makes use of equations (9) and (10) with $\Delta m_{SP} = \beta = 0$) almost unaltered and does not give any improvement in the quality of the fit as is inferred from the fact that the value of the reduced sum χ_r^2 of deviation squares defined as $\chi_r^2 = \chi^2/(N - N_{par})$, where N is the total number of data points in a given temperature interval and N_{par} is the number of free fitting parameters, is not significantly altered. This implies that the accuracy with which magnetization could be determined from FMR measurements in the present case does not suffice to make an unambiguous separation of SW and SP contributions to Δm possible. The optimum values of the parameters that yielded the best theoretical fits to the Δm data for the alloys in question are displayed in table 1. The best theoretical fits so obtained are represented by continuous curves in the M_S versus T plot shown in figure 8. It is observed that the calculated curves provide a very good fit to the data in the entire temperature range, except in the case of alloys with $x \leqslant 2$ at $T < T_{RE}$ where the experimental data deviate considerably from the calculated curves. A steeper increase in $M_S(T)$ for such alloys as the temperature is lowered below T_{RE} than that expected on the basis of theoretical fits attempted at temperatures in the range $T_{RE} \lesssim T \lesssim 0.9T_C$ indicates softening of SW modes at $T \lesssim T_{RE}$. This is so because $M_S(T)$ for $T \lesssim T_{RE}$ can be fitted to equation (10) with a reduced value (compared with that for $T > T_{RE}$) of $D(T) = D(0)$ and β set equal to zero.

Table 1. Magnetic and spin-wave parameters for a-$Fe_{90-x}Co_xZr_{10}$ alloys. The numbers in parentheses denote the estimated uncertainty in the least significant figure.

Co concentration x	$M(0)$ (G)	T_C (K)	$D(0)$ (meV Å^2)	D_2 (10^{-6} K^{-2})	$D(0)/T_C$ (meV Å^2 K^{-1})
0	950(10)	238.50(15)	32(4)	1.819(15)	0.13(3)
1	990(10)	254.50(15)	43(4)	4.837(15)	0.17(3)
2	1002(10)	283.50(20)	51(4)	4.612(15)	0.18(3)
4	987(10)	335.00(20)	71(4)	4.290(15)	0.21(3)
6	1027(10)	376.50(15)	76(4)	2.830(15)	0.20(3)
8	1060(10)	419.50(15)	83(4)	1.940(15)	0.20(3)
10	1103(10)	462.50(20)	90(4)	2.270(15)	0.19(3)
18	1231(10)	683.33(25)	123(6)	1.240(15)	0.18(3)

4. Discussion

Table 2 compares the values of the coefficients a and b of the M_S and M_S^2 terms, respectively, in equation (7) for different Co concentrations. The dominance of the M_S-squared term over the term linear in M_S indicates that multiple-magnon scattering processes dominate over the two-magnon processes which are important for $x \lesssim 2$ only. It is also expected that such scattering processes depend very sensitively on the thermal history of the material. Since

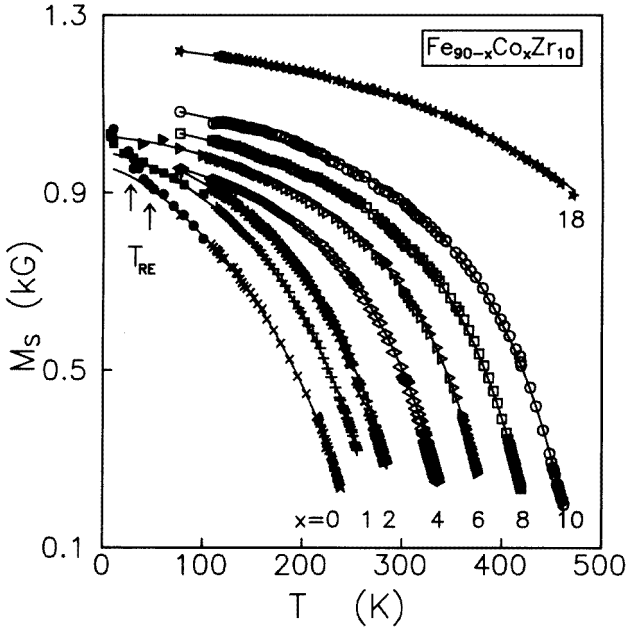

Figure 8. Temperature dependence of saturation magnetization M_S deduced from the lineshape analysis for a-$Fe_{90-x}Co_xZr_{10}$ alloys. The continuous curves through the data points are the best LS fits to the data based on equations (9)–(16) of the text.

exactly identical preparation conditions cannot be ensured in the melt-quenching technique, differences in the thermal histories for different concentrations are bound to occur with the result that ΔH_0 does not exhibit any systematic trend with Co concentration. Heinrich *et al* [19] have shown that the damping parameter $\lambda \propto N(E_F)$, the density of states at the Fermi level, for crystalline ferromagnets and $N(E_F)$ has a very weak or no discernible dependence on temperature. Therefore, it is not surprising that λ is independent of temperature in the present case. The unusually large value of λ for the alloy with $x = 0$ also follows from the fact that $N(E_F)$ has a value as high as 4.4 states eV^{-1}/atom as inferred from the low-temperature specific heat measurements [30] on a-$Fe_{90-x}Zr_{10+x}$ alloys. Such a large value of $N(E_F)$ for a-$Fe_{90}Zr_{10}$ has also been obtained from a more direct method such as ultraviolet photoemission spectroscopy [31]. Consistent with the result that $N(E_F)$ falls rapidly with increasing Co concentration [32] for the alloys under consideration, λ decreases with increasing x (figure 6).

The maxima at low temperatures in $\Delta H_{pp}(T)$ (figure 7) are characteristic of many RE systems [20, 23, 26]. Although it has been suggested earlier that these maxima may be identified with the RE temperatures [23], the present results do not support such a conclusion. The alloys in the a-$Fe_{90-x}Co_xZr_{10}$ series that exhibit RE behaviour possess T_{RE}-values (deduced from low-field magnetization measurements) that are much higher than the T_{max}-values deduced from the LS fits and any coincidence between the two could be fortuitous. Within the framework of the model of infinite FM matrix plus finite FM spin clusters [8–10], the exponential increase in ΔH_{pp} at low temperatures for the alloys with $x \leqslant 2$ may be explained in terms of a theory proposed by Continentino [33]. In this theory, the magnetic two-level systems (TLSs) are assumed to describe the *finite* spin clusters which coexist with the infinite FM cluster and interact with it through a term of the

Table 2. Values of λ, a and b obtained from a least-squares fit to the $\Delta H_{pp}(T)$ data based on equations (6) and (7) of the text.

Co concentration x	λ (10^8 s^{-1})	a (10^{-8})	b (10^{-4} G^{-1})
0	5.1(2)	150.0(10)	0.8(3)
1	4.7(2)	332.0(10)	2.1(2)
2	3.7(2)	9.0(2)	1.7(2)
4	2.6(2)	1.9(2)	1.4(2)
6	2.6(2)	1.8(2)	2.2(2)
8	2.0(2)	1.6(2)	1.5(3)
10	2.1(2)	1.6(2)	2.2(2)
18	1.5(2)	1.1(2)	1.2(2)

form $H_{int} = J(\boldsymbol{\sigma}\cdot\boldsymbol{S}) + \mathcal{D}(\boldsymbol{\sigma}\times\boldsymbol{S})$ in the Hamiltonian

$$\mathcal{H} = \sum_k \epsilon_k a_k^+ a_k + H_{int} \tag{18}$$

where $\epsilon_k = \Delta + D_0k^2$ is the energy of the SWs with stiffness D excited in the infinite cluster while the 'average' coupling constants J and $\mathcal{D}$ describe the effective isotropic exchange and anisotropic Dzyaloshinskii–Moriya (DM) type of interactions between the spins $\boldsymbol{\sigma}$ (Pauli matrices) of the finite clusters and the spins $\boldsymbol{S}$ of the infinite cluster. By making allowance for the fact that the coupling of the infinite cluster with a TLS, although weak, provides an additional relaxation channel for the energy absorbed by the infinite cluster from the microwave field, Continentino arrives at two contributions to the FMR linewidth. The first, called the *resonant* contribution, arises from the interaction between TLSs mediated by SWs (magnons) excited in the infinite cluster by the microwave field and is controlled by the *transverse* relaxation time of the TLS. The second contribution to ΔH_{pp}, called the *relaxation* contribution, is due to a modulation of the population of the states accessible to the finite clusters by the SWs propagating in the infinite cluster. For the range of temperatures covered in the present experiments and the microwave frequency used (about 9.23 GHz), the resonant contribution to ΔH_{pp} is expected to be negligibly small compared with the relaxation contribution. Assuming that the density of states of TLSs per unit volume and unit energy has a constant value of n_0 and that the finite clusters relax through the energy barriers, which are distributed according to the relation

$$P(V) = (1/V_0)\exp(-V/V_0) \tag{19}$$

by the thermal activation process, the *relaxation* contribution to the excess linewidth in the limit $\omega\tau_0 \ll 1$ and $k_BT < V_0$ is given by

$$\Delta\Gamma_{rel}(T) = \Gamma(T) - \Gamma_0 = \Gamma_1(T/T_0)\exp(-T/T_0) \tag{20}$$

with

$$\Gamma_1 = \frac{2\pi S n_0}{h\gamma N_0}\frac{\mathcal{D}}{\ln(\omega\tau_0)} \tag{21}$$

and

$$T_0 = V_0/(k_B\ln(\omega\tau_0)). \tag{22}$$

In equations (20)–(22), ω is the frequency of the SWs excited in the infinite cluster (which is the same as the frequency $\nu = \omega/2\pi$ of the applied microwave field), N_0 is the number of spins per unit volume in the infinite FM cluster, T_0 is the temperature at

which the finite clusters freeze in random orientations, and τ_0, defined by the relation $\tau = \tau_0 \exp(V/k_BT)\,\mathrm{sech}(E/2k_BT)$ which involves the *longitudinal* relaxation time of the TLS and the activation energy V, is the inverse of an attempt frequency. Note that equation (20), which corresponds to the case when $n = 1$ in equation (8), closely reproduces the observed variation in ΔH_{pp} with temperature for $T \lesssim 200$ K in the case of alloys with $x \leqslant 2$ (figure 7). Considering the fact that an exponential distribution of energy barriers (equation (19)), assumed to derive equations (20)–(22), is a direct consequence [34] of the asymptotic form for the cluster size distribution $f(s) \propto \exp[-(s/s_\xi)^{2/3}]$ as predicted by the percolation theory [35] for a three-dimensional system above the percolation threshold, the quantity V_0 (and hence T_0 through equation (22)) is directly related to the *characteristic* cluster size s_ξ. Thus, according to this model, V_0 and T_0 decrease progressively as the increase in the Co concentration reduces the size of finite clusters. This offers a simple explanation for the progressive suppression of the exponential increase in $\Delta H_{pp}(T)$ at low temperatures (and hence of the RE behaviour) as x is increased with the interval $0 \leqslant x \leqslant 4$ (figure 7).

Although equation (20) does provide a quantitative description of $\Delta H_{pp}(T)$ in the temperature range 10 K $\lesssim T \lesssim$ 200 K (figure 7) for the alloys exhibiting RE behaviour, the theory due to Continentino [33] has some obvious limitations. For instance, contrary to our observation that $\Delta H_{pp}(T)$ follows the temperature variation predicted by equation (20) up to temperatures as high as $3T_{RE}$, equation (20) is strictly valid only at very low temperatures, i.e. for $T \ll V_0/k_B$. Moreover, this theory predicts a large shift in the line centre concomitant with increased linewidths, which has not been observed in many random spin systems including those studied by us. Systematic studies of frequency dependence in concentrated amorphous SG systems [36] have revealed that Γ_1 exhibits a 'resonant anomaly' as a function of frequency and, for very low temperatures, Γ_1 increases roughly by a factor of 5 in contrast with the theoretical prediction that Γ_1 is frequency independent. This could imply that the distribution functions of the TLS might be more complicated than assumed in the theory due to Continentino. Hence, a more detailed microscopic theory of linewidths in these systems is called for.

A plot of $D(0)$ against T_C, the Curie temperature (determined from the scaling analysis [37]), is depicted in figure 9, which also includes the predictions of the three-dimensional Heisenberg model [38] which either takes into account the exchange interactions between the nearest neighbours (NNs) only (broken straight line) or considers both the NN and the next-nearest-neighbour (NNN) exchange interactions (solid straight line). The figure also includes $D(0)$ and T_C data available in the literature on other similar glassy alloy systems. In accordance with the theoretical predictions [38], the $D(0)$-values for amorphous FM alloys, when plotted against T_C, fall on a straight line represented by the equation

$$D(0) = D_0 + mT_C \tag{23}$$

where $m = 0.144$ meV Å^2 K^{-1} and D_0 is either finite or zero, depending on whether the exchange interactions extend beyond the NN distance or not. It has been observed that the values of $D(0)$ for a-(Fe,M)–B alloys (M = Cr, Mn or W) [12, 39, 40] fall on a straight line with $m = 0.144$ meV Å^2 K^{-1} passing through the origin whereas the $D(0)$-values for the a-(Fe,Ni)–M′ alloys (M′ = P, B, Si or Al) [38, 41, 42] fall on another straight line which is parallel to the earlier line but with a finite intercept $D_0 \simeq 24 \pm 3$ meV Å^2 K^{-1}. Thus, the competing interactions in the former set of alloys confine the direct exchange interactions to NNs only whereas in the latter set, due to the absence or suppression of competing interactions, the direct exchange interactions involve not only the NNs but also the NNNs. Now that the $D(0)$-values for the concentrations $y = 0$ ($x = 0$ in a-$Fe_{90-x}Co_xZr_{10}$) and 1

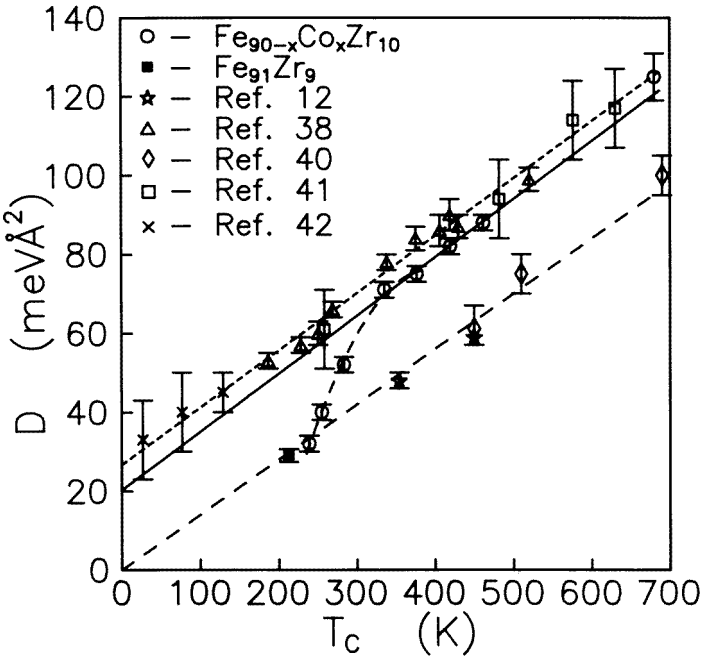

Figure 9. Variation in the SW stiffness coefficient D with T_C for a-$Fe_{90-x}Co_xZr_{10}$ alloys. The figure also shows data taken from literature for some amorphous alloys with and without the presence of competing interactions. The broken and continuous straight lines through the data points are LS fits to the data based on equation (23) of the text with $m = 0.144$ meV Å^2 K^{-1}.

in the a-$Fe_{90+y}Zr_{10-y}$ alloy series fall on the straight line passing through the origin, this implies that the direct exchange interactions in these alloys are being confined to the NNs only. When an increasing amount of Fe is replaced by Co, the competing interactions are progressively suppressed, the alloys become relatively more homogeneous and the direct exchange interactions for $x \geqslant 6$ now extend to NNNs also. In the intermediate-Co-concentration range ($2 \leqslant x \leqslant 4$), a crossover from the short-ranged (NN distance) to the long-ranged (NNN distance) exchange takes place.

An alternative explanation can be offered for the observations mentioned above in terms of the model of infinite FM matrix plus finite FM clusters [8–10], which is applicable to glassy FM systems only. In this model, the spin system for $T \leqslant T_C$ is composed of an infinite three-dimensional FM network or matrix (high-density bulk) and finite spin clusters (microscopic low-density pockets) that are embedded in this matrix such that the average NN distance between magnetic atoms in the low-density pockets is appreciably *greater* than in the remaining bulk. Therefore, the FM coupling between the spins in the low-density regions is much stronger than that between the spins in the high-density bulk. Owing to a considerable mismatch in the NN spacings within the zones that separate these microscopic low-density regions from the high-density bulk, there are large 'quenched-in' *local* stresses in such zones. Random fluctuations in the NN distances within these zones around the critical distance at which the exchange integral changes sign in the Bethe–Slater curve give rise to competing interactions. An additional contribution to competing interactions arises from strong *magnetostrictive* coupling between the local 'quenched-in'

stresses and spins in the buffer or frustration zones surrounding the low-density regions. The frustration zones thus tend to isolate the finite spin clusters from the FM matrix. The isolation is, however, not complete in that a residual but weak interaction does exist between the spin clusters and FM matrix. As the temperature is lowered below T_C, spin clusters start to freeze in random orientations at a certain temperature T_{RE} (large clusters at higher temperatures and smaller clusters at lower temperatures) due to the Ruderman–Kittel–Kasuya–Yosida (RKKY) coupling between them. Frozen clusters impose a random anisotropy field (RAF) on the spins contained in the FM matrix. Although the RAF grows in strength with decreasing temperature, it is unable to destroy the long-range FM order in the matrix because the coupling between the finite clusters and the FM matrix is *weak*. However, such a coupling does not prevent the frozen clusters from polarizing the spins in the FM matrix (surrounding the frustration zones) along their net magnetization directions. As a consequence, the equilibrium configuration of spins in the FM matrix is the one in which the FM spins are *canted* with respect to one another. The canting angle, although small, increases slowly as the clusters smaller in size freeze in random orientations when the temperature is lowered below T_{RE}. The exchange interaction between the spins in the FM matrix weakens progressively as the canting angle increases and hence the SW modes soften for $T \lesssim T_{RE}$. Concomitance of the reduced value of the SW stiffness with thermomagnetic and thermoremanent effects for $T \lesssim T_{RE}$ thus implies that the RE state is a *mixed* state in which the (*canted*) FM long-range order coexists with the cluster SG order. Moreover, the finding that the upturn in $\Delta H_{pp}(T)$ for RE alloys with $x \leqslant 2$ does not occur at T_{RE}, the temperature which marks the onset of strong irreversibility in low-field magnetization, but at $T \simeq 3T_{RE}$ implies that all the finite clusters do not start to freeze in random orientations at T_{RE}; instead the largest cluster begins to freeze at $T \simeq 3T_{RE}$ and increasingly smaller clusters freeze at lower temperatures. This inference is further supported by the observation that the zero-field-cooled and field-cooled ($H = 3$ kOe) $H_{res}(T)$ and $\Delta H_{pp}(T)$ curves bifurcate at $T \simeq 3T_{RE}$ for the alloys with $x \leqslant 2$ (a typical behaviour is depicted in figure 10). Thus, in conformity with our recent Mössbauer results [3], the freezing process occurs over a wide temperature range and is a thermally activated process. The effect of partially replacing Fe with Co on the RE behaviour can be explained in terms of this model as follows. Since the Fe–Co and Co–Co exchange interactions are FM and stronger than Fe–Fe exchange coupling, the addition of Co suppresses the competing interactions in the frustration zones surrounding the finite clusters and this leads to a breaking-up of the finite clusters into smaller clusters and even a merging of some of them with the infinite matrix, while the surviving clusters are better isolated from the FM matrix. Consequently, as the Co concentration increases, the number of spins constituting the FM matrix increases at the expense of those forming the clusters, the spins within the FM matrix tend towards a collinear configuration, the spin system becomes more homogeneous and all the features that are characteristic of RE behaviour, e.g. exponential increase in ΔH_{pp} and confinement of direct exchange interactions to the NNs only, are progressively suppressed. The net result of all these considerations is that the magnitude of saturation magnetization at any given value of reduced temperature T/T_C *increases* with increasing Co concentration, as is borne out by the data presented in figure 11.

5. Summary and conclusions

Detailed FMR measurements on a-$Fe_{90-x}Co_xZr_{10}$ ($0 \leqslant x \leqslant 18$) have been performed in the temperature range 10–500 K in the horizontal-parallel and vertical-parallel sample configurations at a fixed microwave frequency of about 9.23 GHz. From a detailed analysis

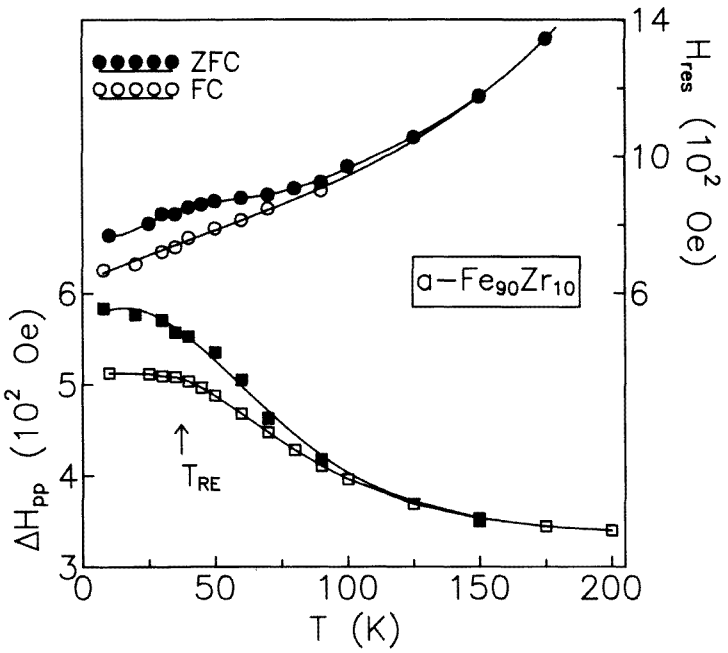

Figure 10. Temperature dependence of H_{res} and ΔH_{pp} in the low-temperature region for a-$Fe_{90}Zr_{10}$ alloy. The full and open symbols represent the zero-field-cooled and field-cooled experimental runs, repectively. The continuous curves through the data points serve as guides to the eye.

of the linewidth and magnetization data deduced from the lineshape analysis, the following inferences can be drawn.

(i) The frequency-independent part ΔH_0 of ΔH_{pp} has its origin in the two-magnon and multiple-magnon scattering mechanisms. The dominance of the M_S^2 term over the M_S term, especially for alloys with $x > 2$, implies that in these compositions multiple-magnon scattering processes are important. ΔH_0 depends very sensitively on the thermal history of the sample and does not show any systematic variation with Co concentration.

(ii) Linewidths for $x = 0$, 1 and 2 increase exponentially at low temperatures and go through a maximum, which is a *characteristic* feature of RE systems. This increase is qualitatively explained in terms of the theory proposed by Continentino based on the model of infinite FM cluster plus finite-clusters. However, some caution has to be exercised while interpreting FMR data using this theory. In contradiction to the predictions of this theory, the linewidth data obey equation (9) up to temperatures as high as $3T_{RE}$ and Γ_1 exhibits a 'resonant' anomaly as a function of frequency [36]. Hence, a more detailed microscopic theory of linewidths in these systems is called for.

(iii) The exponential increase in ΔH_{pp} at low temperatures is completely suppressed for alloys with $x > 4$, implying that the RE behaviour is suppressed for higher Co concentrations.

(iv) The Gilbert damping parameter λ ($\propto N(E_F)$) is temperature independent and decreases with increasing Co concentration, a result which follows from the fact that $N(E_F)$ has a weak or no discernible dependence on temperature and falls rapidly with increasing

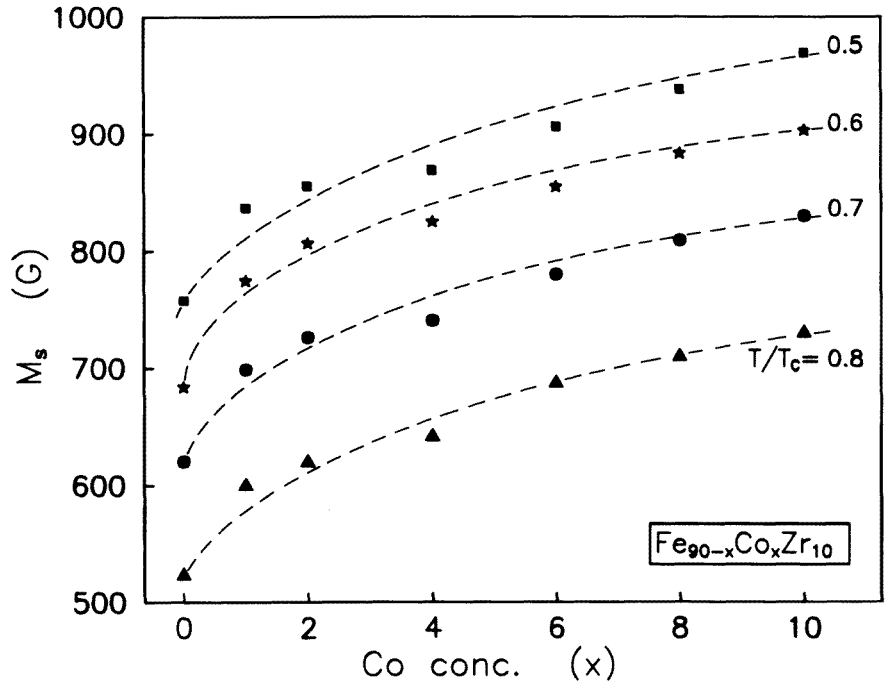

Figure 11. Co concentration dependence of saturation magnetization M_S at a few representative values of reduced temperature T/T_C.

x. The Landé splitting factor g is also temperature independent but has a concentration-independent value of 2.07 ± 0.02.

(v) While the dominant contribution to thermal demagnetization is from SW excitations, additional contributions from SP excitations may not be ruled out. The SW stiffness coefficient $D(0)$ renormalizes with temperature in accordance with the predictions of the itinerant-electron model.

(vi) The SW modes soften as the temperature is lowered through T_{RE}.

(vii) Competing interactions in the parent alloy a-$Fe_{90}Zr_{10}$ confine the direct exchange interactions to the NNs only but the replacement of Fe with Co ($x > 4$) results in the suppression of competing interactions and the range of direct exchange now extends to NNNs also.

(viii) Finite spin clusters in the RE alloys with $x \leqslant 2$ freeze in random orientations over a wide temperature range and the freezing process is a thermally activated process.

(ix) The model of finite FM spin clusters plus infinite FM matrix provides a satisfactory explanation for all the diverse aspects of the FMR results.

Acknowledgments

The authors are grateful to Dr M D Sastry and Dr R M Kadam, Radiochemistry Division, Bhabha Atomic Research Centre, Bombay, India, for extending their facilities for the low-temperature FMR work.

References

[1] Kaul S N 1983 *Phys. Rev.* B **27** 6923
[2] Deppe P, Fukamichi K, Li F S, Rosenberg M and Sostarich M 1984 *IEEE Trans. Magn.* **20** 1367
[3] Kaul S N, Siruguri V and Chandra G 1992 *Phys. Rev.* B **45** 12 343
[4] Krishnan R, Rao K V and Liebermann H H 1984 *J. Appl. Phys.* **55** 1823
[5] Beck W and Kronmüller H 1985 *Phys. Status Solidi* b **132** 449
[6] Fish G E and Rhyne J J 1987 *J. Appl. Phys.* **61** 454
[7] Kaul S N 1991 *J. Phys.: Condens. Matter* **3** 4027
[8] Kaul S N 1984 *IEEE Trans. Magn.* **20** 1290
[9] Kaul S N 1985 *J. Magn. Magn. Mater.* **53** 5
[10] Kaul S N 1988 *J. Phys. F: Met. Phys.* **18** 2089
[11] Fernandez-Baca J A, Rhyne J J, Fish G E, Hennion M and Hennion B 1990 *J. Appl. Phys.* **67** 5223
[12] Kaul S N and Mohan Babu T V S M 1989 *J. Phys.: Condens. Matter* **1** 8509
[13] Siruguri V, Mohan Ch V and Kaul S N 1991 *Solid State Phys. (India)* **34C** 121
[14] Kaul S N and Siruguri V 1992 *J. Phys.: Condens. Matter* **4** 505
[15] Kaul S N and Siruguri V 1987 *J. Phys. F: Met. Phys.* **17** L255
[16] Ounadjela K, Suran G and Machizaud F 1989 *Phys. Rev.* B **40** 570
[17] Webb D J and Bhagat S M 1987 *J. Magn. Magn. Mater.* **42** 109
[18] Heinrich B, Fraitova D and Kambersky V 1967 *Phys. Status Solidi* **23** 501
[19] Heinrich B, Myrtle K, Rudd J M, Cochran J F and Hasegawa R 1983 *J. Magn. Magn. Mater.* **31–4** 1597
[20] Spano M L and Bhagat S M 1981 *J. Magn. Magn. Mater.* **24** 143
[21] Cochran J F, Myrtle K and Heinrich B 1982 *J. Appl. Phys.* **53** 2261
[22] Cochran J F, Heinrich B and Hasegawa R 1985 *J. Appl. Phys.* **57** 3690
[23] Coles B R, Sarkissian B V B and Taylor R H 1978 *Phil. Mag.* B **37** 789
[24] Park M J, Bhagat S M, Manheimer M A and Moorjani K 1986 *J. Magn. Magn. Mater.* **59** 287
[25] Bhagat S M, Spano M L and Lloyd J N 1981 *Solid State Commun.* **38** 261
[26] Rosenbaum T F, Rupp L N Jr, Thomas G A, Walsh W M Jr, Chen H S, Banavar J R and Littlewood P B 1982 *Solid State Commun.* **42** 725
[27] Keffer F 1966 *Encyclopaedia of Physics* vol XVIII, part 2, ed H P J Wijn (Berlin: Springer) p 1
[28] Mathon J and Wohlfarth E P 1968 *Proc. R. Soc.* A **302** 409
[29] Kaul S N and Babu P D 1992 *J. Phys.: Condens. Matter* **4** 6429
[30] Mizutani U, Matsuura M and Fukamichi K 1984 *J. Phys. F: Met. Phys.* **14** 731
[31] Neddermeyer H and Paul Th 1987 *Phys. Rev.* B **36** 4148
[32] Rosenberg M, Hardebusch U, Schöne-Warnefeld A, Wernhardt R and Fukamichi K 1988 *J. Phys. F: Met. Phys.* **18** 259
[33] Continentino M A 1983 *J. Phys. C: Solid State Phys.* **16** L71; 1983 *Phys. Rev.* B **27** 4351
[34] Cohen M H and Continentino M A 1985 *Solid State Commun.* **55** 609
[35] Stauffer D 1979 *Phys. Rep.* **54** 1
[36] Liao S B, Bhagat S M, Manheimer M A and Park M J 1987 *Solid State Commun.* **63** 119
[37] Siruguri V, Babu P D and Kaul S N 1994 *AIP Conf. Proc.* **286** 309
Siruguri V and Kaul S N 1996 *J. Phys.: Condens. Matter* **8** 4567
[38] Kaul S N 1983 *Phys. Rev.* B **27** 5761
[39] Dey S, Gorres U, Nielsen H J V, Rosenberg M and Sostarich M 1980 *J. Physique Coll.* **41** C8 678
[40] Soumura T, Takeda K, Wakano T, Terasawa K and Maeda T 1986 *J. Magn. Magn. Mater.* **58** 202
[41] Birgeneau R J, Tarvin J A, Shirane G, Gyorgy E M, Sherwood R C, Chen H S and Chien C L 1978 *Phys. Rev.* B **18** 2192
[42] Hilscher G, Haferl R, Kirchmayer K, Mueller M and Guntherödt H J 1981 *J. Phys. F: Met. Phys.* **11** 2429